J|A|C|S
ARTICLES
Published on Web 04/04/2003

Comparison of Nanotube Structures Constructed from α-, β-, and γ-Cyclodextrins by Potential-Controlled Adsorption

Akihiro Ohira, Masayo Sakata, Isao Taniguchi, Chuichi Hirayama, and Masashi Kunitake*

Contribution from the Department of Applied Chemistry & Biochemistry, Faculty of Engineering, Kumamoto University, 2-39-1 Kurokami, Kumamoto 860-8555, Japan

Received November 13, 2002; E-mail: kunitake@chem.kumamoto-u.ac.jp

Abstract: "Nanotube" structures of the α-, β-, and γ-cyclodextrins (CyD's), which are similar to that of CyD−polyrotaxane, were constructed by potential-controlled adsorption onto Au(111) surfaces in sodium perchlorate solution without a threaded polymer. CyD molecules adsorbed randomly on bare Au(111) surfaces without potential control and the desorption of CyD's from Au surfaces was observed at a negative potential of less than −0.60 V versus SCE. On the other hand, in the specific range between these potentials, ordered molecular arrays with "nanotube" structures of the CyD's (α-, β-, and γ-CyD) were observed on Au(111). The range of potentials for formation of the "nanotube" structures of α-, β-, and γ-CyD was from −0.15 to −0.20 V, from −0.25 to −0.45 V, and from −0.22 to −0.45 V, respectively. β- and γ-CyD require a more negative potential for adsorption-induced self-organization (AISO) than α-CyD in order to weaken adsorption and induce self-organization. Furthermore, we have succeeded in the visualization of the dynamic process in solution, such as the self-ordering, and the destruction of the nanotube structure. These results indicate that control of the electrode potential facilitates management of the delicate balance of various interactions, resulting in the formation of two-dimensional supramolecular structures on the substrates.

1. Introduction

Recent progress in high-resolution STM imaging[1] has allowed the visualization of the arrangements, orientations, and even inner structures of molecules in air,[2] in ultrahigh vacuum (UHV),[3] and in solution.[4−7,9] Recently, applications of this technique have focused on the self-organization of highly ordered molecular adlayers and/or two-dimensional (2D) supramolecular aggregations rather than the epitaxial arrangements of surface chemistry.[1] The observation of 2D molecular architecture by STM has led to a "visual" understanding of

(1) (a) Itaya, K. *Prog. Surf. Sci.* **1998**, *58*, 121−248. (b) Lipokowski, J., Ross P. N., Eds. *Imaging of Surfaces and Interfaces*; VCH Publishers: New York, 1999. (c) Poggi, M. A.; Bottomley, L. A.; Lillehei, P. T. *Anal. Chem.* **2002**, *74*, 2851−2862.

(2) (a) Heckl, W. M.; Kallury, K. M. R.; Thompson, M.; Gerber, C.; Horber, H. J. K.; Binnig, G. *Langmuir* **1989**, *5*, 1433−1435. (b) Snyder, S. R.; White, H. S.; Lopez, S.; Abruna, H. D. *J. Am. Chem. Soc.* **1990**, *112*, 1333−1337. (c) Widrig, C. A.; Alves, C. A.; Porter, M. D. *J. Am. Chem. Soc.* **1991**, *113*, 2805−2810. (d) Kim, Y.-T.; Bard, A. J. *Langmuir* **1992**, *8*, 1096−1102. (e) Luttrull, D. K.; Graham, J.; DeRose, J. A.; Gust, D.; Moore, T. A.; Lindsay, S. M. *Langmuir* **1992**, *8*, 765−768. (f) Kim, Y.-T.; McCarley, R. L.; Bard, A. J. *J. Phys. Chem.* **1992**, *96*, 7416−7421. (g) Viswanathan, R.; Zasadzinski, J. A.; Schwartz, D. K. *Science* **1993**, *261*, 449−452. (h) Li, M. Q. *Appl. Phys. A: Mat. Sci. Process.* **1999**, *A68*, 255−258.

(3) (a) Poirier, G. E.; Pylant, E. D. *Science* **1996**, *272*, 1145−1148. (b) Chiang, S. *Chem. Rev.* **1997**, *97*, 1083−1096. (c) Jung, T. A.; Schlittler, R. R.; Gimzewski, J. K. *Nature* **1997**, *386*, 696−699. (d) Soriaga, M. P.; Itaya, K.; Stickney, J. L. *Electrochem. Nanotechnol.* **1998**, 267−276. (e) Gimzewski, J. K.; Joachim, C.; Schlittler, R. R.; Langlais, V.; Tang, H.; Johannsen, I. *Science* **1998**, *281*, 531−533. (f) Gimzewski, J. K.; Joachim, C. *Science* **1999**, *283*, 1683−1688. (g) Tanaka, H.; Hamai, C.; Kanno, T.; Kawai, T. *Surf. Sci.* **1999**, *432*, L611−L616. (h) Taniguchi, M.; Nakagawa, H.; Yamagishi, A.; Yamada, K. *Surf. Sci.* **2000**, *454*−*456*, 1005−1009. (i) Bohringer, M.; Schneider, W.-D; Berndt, R. *Angew. Chem., Int. Ed.* **2000**, *39*, 792−795. (j) Hla, S.-W.; Meyer, G.; Rieder, K.-H. *ChemPhysChem* **2001**, *2*, 361−366. (k) Yokoyama, T.; Yokoyama, S.; Kamikado, T.; Okuno, Y.; Mashiko, S. *Nature* **2001**, *413*, 619−621. (l) Poirier, G. E. *Phys. Rev. Lett.* **2001**, *86*, 83−86. (m) Weckesser, J.; De Vita, A.; Barth, J. V.; Cai, C.; Kern, K. *Phys. Rev. Lett.* **2001**, *87*, 096101-1−096101-4. (n) Ackinger, M.; Griessl, S.; Heckl, Wolfgang M.; Hietschold, M. *J. Phys. Chem. B* **2002**, *106*, 4482−4485. (o) Barth, J. V.; Weckesser, J.; Trimarchi, G.; Vladimirova, M.; De Vita, A.; Cai, C.; Brune, H.; Gunter, P.; Kern, K. *J. Am. Chem. Soc.* **2002**, *124*, 7991−8000.

(4) (a) Rabe, J. P.; Buchholz, S. *Science* **1991**, *253*, 424−427. (b) Schwinn, T.; Gaub, H. E.; Rabe, J. P. *Supramol. Sci.* **1994**, *1*, 85−90. (c) Cincotti, S.; Rabe, J. P. *Supramol. Sci.* **1994**, *1*, 7−10. (d) Heinz, R.; Stabel, A.; DeSchryver, F. C.; Rabe, J. P. *J. Phys. Chem.* **1995**, *99*, 505−507. (e) Heinz, R.; Stabel, A.; DeSchryver, F. C.; Rabe, J. P. *J. Phys. Chem.* **1995**, *99*, 8690−8697. (f) EichhorstGerner, K.; Stabel, A.; Moessner, G.; Declerq, D.; Valiyaveettil, S.; Enkelmann, V.; Mullen, K.; Rabe, J. P. *Angew. Chem., Int. Ed. Engl.* **1996**, *35*, 1492−1495. (g) DeFeyter, S.; Gesquiere, A.; Abdel-Mottaleb, M. M.; Grim, P. C. M.; DeSchryver, F. C. *Acc. Chem. Res.* **2000**, *33*, 520−531. (h) Samorí, P.; Jäckel, F.; Ünsal, Ö.; Godt, A.; Rabe, J. P. *Chem. Phys. Chem.* **2001**, *7*, 461−464. (i) Giancarlo, L. C.; Fang, H.; Rubin, S. M.; Bront, A. A.; Flynn, G. W. *J. Phys. Chem. B* **1998**, *102*, 10255−10263.

(5) (a) Kunitake, M.; Akiba, U.; Batina, N.; Itaya, K. *Langmuir* **1995**, *11*, 2337−2340. (b) Batina, N.; Kunitake, M.; Itaya, K. *J. Electroanal. Chem.* **1996**, *405*, 245−250. (c) Kunitake, M.; Akiba, U.; Batina, N.; Itaya, K. *Langmuir* **1997**, *13*, 1607−1615. (d) Ogaki, K.; Batina, N.; Kunitake, M.; Itaya, K. *J. Phys. Chem.* **1996**, *100*, 7185−7190.

(6) (a) Ohira, A.; Ishizaki, T.; Sakata, M.; Kunitake, M.; Taniguchi, I.; Hirayama, C. *J. Electroanal. Chem.* **1999**, *472*, 163−167. (b) Ohira, A.; Ishizaki, T.; Sakata, M.; Taniguchi, I.; Hirayama, C.; Kunitake, M. *Colloids Surf., A* **2000**, *169*, 27−33. (c) Sakai, T.; Ohira, A.; Sakata, M.; Hirayama, C.; Kunitake, M. *Chem. Lett.* **2001**, 782−783. (d) Pan, G.-B.; Wan, L.-J.; Zheng, Q.-Y.; Bai, C.-L.; Itaya, K. *Chem. Phys. Lett.* **2002**, *359*, 83−88. (e) Ohira, A.; Sakata, M.; Hirayama, C.; Kunitake, M. *Org. Biomol. Chem.* **2003**, *1*, 251−253.

(7) Ishikawa, U.; Ohira, A.; Sakata, M.; Hirayama, C.; Kunitake, M. *Chem. Commun.* **2002**, 2652−2653.

(8) Hooks, D. E.; Fritz, T.; Ward, M. D. *Adv. Mater.* **2001**, *13*, 227−241.

(9) (a) Cunha, F.; Tao, N. J. *Phys. Rev. Lett.* **1995**, *75*, 2376−2379. (b) Wandlowski, T.; Lampner, D.; Lindsay, S. M.; *J. Electroanal. Chem.* **1996**, *404*, 215−226. (c) Cunha, F.; Tao, N. J.; Wang, X. W.; Jin, Q.; Duong, B.; D'Agnese, J. *Langmuir* **1996**, *12*, 6410−6418. (d) Wandlowski, Th.; Dretschkow, Th.; Dakkouri, S. A. *Langmuir* **1997**, *13*, 2843−2856. (e) Cunha, F.; Jin, Q.; Tao, N. J.; Li, C. Z. *Surf. Sci.* **1997**, *389*, 19−28. (f) Schweizer, M.; Hagenstrom, H.; Kolb D. M. *Surf. Sci.* **2001**, *490*, L627−636.

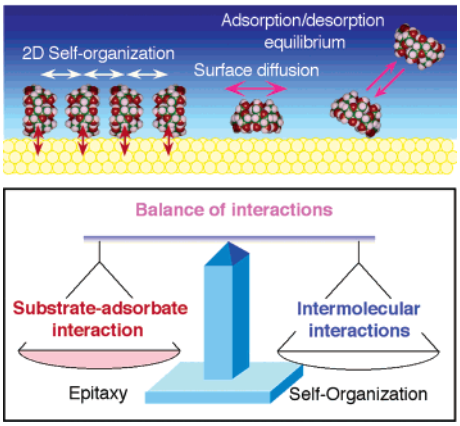

Figure 1. Schematic illustration of the concept for adsorption-induced self-organization.

intermolecular interactions. In the majority of research to date, the preparation and STM observation have been conducted in UHV.[3] Gimzewski and co-workers have demonstrated the relocation and the rotation of a single molecule in the 2D supramolecular structures.[3c,e,f] These movements were achieved using molecules with bulky *tert*-butyl legs to weaken the substrate−adsorbate interaction on Cu(100) surfaces. Yokoyama and co-workers successfully created various arrangements of porphyrine molecules, such as monomeric, trimeric, tetrameric, and extended 1D aggegation like a wire onto an Au surface using low-temperature UHV−STM.[3k] The structures were dependent upon individual intermolecular interactions which were controlled by the number and placement of cyanophenyl substituents on molecules. Recently, the chiral arrangement of molecules on surfaces has also become a hot issue in the field of STM.[3i,m,o] The supramolecular self-organization of 2D chiral species induced by intermolecular interactions has been investigated using low-temperature UHV−STM.[3i,m,o] Generally, the type of substrate, the temperature of the substrate, and the surface coverage (usually less than 1 mL) are carefully set when using UHV−STM equipment to facilitate relatively weak adsorbate−substrate interactions, which allows the induction of self-organization.

On the other hand, Rabe and co-workers have extensively researched the 2D self-organized structure of various molecules having long alkyl chains on highly ordered pyrolytic graphite (HOPG) or molybdenum disulfied (MoS_2) in organic solvent such as phenyloctane.[4a−h] Recently, they have also focused on the molecular arrangements constructed by intermolecular hydrogen bonds.[4f] As another "wet process" methodology to induce self-organization, we have proposed adsorption-induced self-organization (AISO),[5−7] which is based on spontaneous adsorption from a solution onto a substrate and then 2D self-organization on the substrate surface, as shown in Figure 1. It has proven to be a simple and valuable "wet process" methodology for preparing highly ordered molecular adlayers on well-defined surfaces.

In AISO, the key to inducing self-organization is to achieve mild adsorption under controlled conditions similar to those in UHV. If the adsorbate−substrate interaction is too strong, the molecules cannot move around on the substrate surface. On the other hand, when the adsorbate−substrate interaction is too weak, the molecules desorb from the surfaces. Relatively mild adsorption conditions between these extreme states lead to the induction of 2D self-organization of molecules via rapid surface diffusion and acceleration of the adsorption/desorption equilibrium.

The concept of AISO has been reported, for the first time, in 1995;[5a] porphyrin molecules easily self-organize and form highly ordered adlayers on an iodine-modified Au surface (I/Au) but not on a bare Au surface by spontaneous adsorption from solutions. The difference of the adsorption behaviors has been explained by a relatively weaker interaction on I/Au to allow surface diffusion of the molecules. It is clear proof by in situ observation of an ordering process of molecules on I/Au.[5c] Ward and co-workers have discussed in depth about the molecular organization on the solid substrates from the view of epitaxy using various UHV−STM results.[8] In the review, they have also pointed out the significance of the balance of overlayer−substrate and molecule−molecule energies.

To manage adsorbate−substrate interactions, a selection of substrates is important both in UHV and in solution systems. The most suitable substrate for self-organization depends on the type of molecule being adsorbed. The highly ordered adlayers of relatively small aromatic molecules were known to be formed on Pt or Rh in epitaxial fashion. However, among the single crystal metal substrates, generally Cu, Ag, and Au are probably preferable to catalytic surfaces, such as Pt and Rh, as substrates for self-organization of molecules due to the relatively weak adsorption of organic molecules. For another example, it has been reported that highly ordered molecular adlayers of porphyrin[1,5] and crystal violet[5] were formed on iodine-modified Au and Ag surfaces, as we mentioned.

Not only a selection of substrates but also electrochemical potential management would be convenient for AISO in the "wet process", because it allows for precise control of the adsorption strength in units of millivolts.[1b,6,7,9] In previous papers, we have reported the formation of the 2D supramolecular nanotube structures of α- and β-cyclodextrin (CyD)[6a,b] and calix[4]arene[6c] which was achieved by potential-controlled adsorption. In the management of the adsorption strength or surface diffusion of molecules, it is important to understand that electrochemical potential management for the preparation of ordered structures in solution essentially corresponds to the control of the substrate temperature in the UHV preparation.

Potential-controlled in situ STM observation of "order−disorder" and "order−order" phase transitions of adlayers of organic compounds such as DNA bases,[1b,9b] heterocyclic molecules,[1b,9a,c,d] and thiol molecules[9e] have been reported. Tao and co-workers have discussed in detail about an "order−disorder" phase transition of 2,2′ bipyridine on Au(111).[1b,9a,c] They have pointed out that phase transition was induced by a change of surface charge density in the function of electrode potential. Just recently, we have succeeded in constructing a 2D molecular network of trimesic acid on Au(111) by means of precisely potential-controlled adsorption.[7] Furthermore, an "order−order" phase transition between the network structure and a closed packed structure was also constructed by the control of potential.

As target molecules to construct 2D supramolecular arrangements by AISO, host molecules such as cyclodextrins (CyD's),[6a,b] calixarene,[6c,d] and crown ether were focused on.[6e] Host molecules have attracted attention not only in the field of host−guest chemistry but also in supramolecular chemistry as

Scheme 1. Chemical Structure and Space Filling Models of α-, β-, and γ-CyD. X and Y Indicate the Outside Diameters of the Cavity and Height of CyD, Respectively

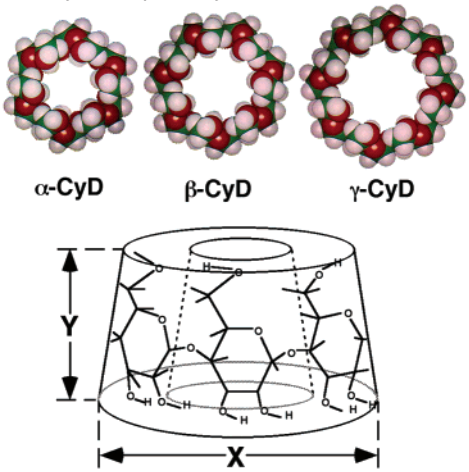

topological supramolecule components.[11,13−16] Among the various host molecules, CyD belongs to a class of naturally occurring cyclic molecules made up of 6−12 glucopyranose units linked through α-1,4 glycosidic bonds.[12] The most common of these macrocyclic oligosaccharides are α-, β-,and γ-CyD which contain six, seven, and eight glucose units, respectively (Scheme 1).

In host−guest chemistry, the CyD's possess an interior hydrophobic cavity that can include a wide variety of guest species.[12] In the past decade, CyD's have also been used as components of supramolecules[11,13−16] such as rotaxanes, catenanes, polyrotaxanes, and so on. CyD−polyrotaxane (Scheme 2a), in which polymers such as poly(ethylene glycol) (PEG) or polyprophyleneglycol (PPG) are threaded into the cavity of the CyD's, have been the focus of much research over the last decade.[15] This was first discovered and reported by Harada and co-workers at 1992. The CyD-nanotube structures prepared by adsorption onto Au surfaces resemble the polyrotaxane structures, as shown in Scheme 2. Furthermore, they have also succeeded in synthesizing the supramolecular structures of "cross-linked CyD nanotubes" without using a threaded polymer.[16]

Scheme 2. Schematic Representation of (a) Polyrotaxane and (b) CyD Nanotube Observed by STM

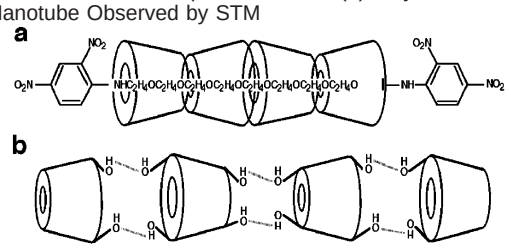

Several STM observations of CyD's have been reported. Shigekawa and co-workers reported STM images of an isolated or partially aggregated α-CyD on MoS_2 and the analogue of α-CyD on adsorbed graphite in air.[17] They have also reported the manipulation of α-CyD molecules in the polyrotaxane by using the STM tip as a "molecular abacus".[17c] In other current research, Liu and co-workers have reported the wire-like polyrotaxane structure of organo-selenium bridged bis(cyclodextrin)s with a calix[4]arene derivative on HOPG by STM in air.[18] We described the formation of the 2D arrays consisting of nanotube structures originating from α- and β-cyclodextrin (CyD) on Au(111) without use of a threaded polymer.[6a,b] The formation of CyD nanotubes was achieved by the potential-controlled adsorption based on AISO.

In this report, we would like to describe the formation of "nanotube" structures of α-, β- and γ-CyD's on Au(111) at controlled electrode potentials based on AISO by means of in situ STM. We demonstrate not only high-resolution STM images of CyD molecules but also the dynamic observation of phase transitions among the "desorption", "self-organization-to-nanotube", and "disordered" states of CyD's.

2. Materials and Methods

2.1. Materials. All solutions were prepared with ultrapure (Milli-Q, SP-TOC, >18.2 MΩ cm^{-1}). $NaClO_4$ (Katayama Chemical Co. Ltd., Japan) was used as an electrolyte solution without further purification. The concentration of the $NaClO_4$ prepared was 10 mM. All CyD's (Kanto Chemical Co. Ltd., Japan) were used. The concentration of the CyD was typically ∼2.0 μM without further purification.

The Au wire (0.8 mm in diameter), of which the purity was 99.999%, was obtained from Tanaka Kikinzoku Co. Ltd., Japan and was used to prepare a single-crystal bead for electrochemical and STM measurements. The Pt wire, which was also 0.8 mm in diameter with a purity of 99.99%, was also obtained from Tanaka Kikinzoku and was used as a counter electrode and/or quasi-reference electrode.

2.2. Cyclic Voltammetry (CV). As the electrolyte solution, a 10 mM $NaClO_4$ aqueous solution was prepared. Well-defined bare Au(111) electrodes, which were prepared by cutting and mechanically polishing the Au single-crystal bead, were used for voltammetric measurements, as described in previous papers.[6a−c] The Au(111) electrodes were annealed in an H_2-O_2 flame and quenched in pure water saturated with H_2. The electrodes were transferred into an electrochemical cell filled with 10 mM $NaClO_4$ aqueous solution containing CyD aerated with N_2 gas. All potentials are quoted with respect to a saturated calomel electrode (SCE).

2.3. Electrochemical Scanning Tunneling Microscopy (EC−STM). In situ STM measurements were carried out with a Nanoscope

(10) Lipokowski, J.; Ross P. N., Eds. *Adsorption of Molecules at Metal Electrodes*; VCH Publishers: New York, 1992.
(11) Lehn, J.-M. *Supramolecular Chemistry*; VCH Publishers: Weinheim, 1995.
(12) Bender, M.; Komiyama, M. *Cyclodextrin Chemistry*; Springer: Berlin, 1976.
(13) (a) Sauvage, J.-P. *Acc. Chem. Res.* **1998**, *31*, 611−619. (b) Balzani, V.; Gomez-Lopez, M.; Stoddart, J. F. *Acc. Chem. Res.* **1998**, *31*, 405−411. (c) Nepogodiev, S. A.; Stoddart, J. F. *Chem. Rev.* **1998**, *98*, 1959−1976. (d) Hoshino, T.; Miyauchi, M.; Kawaguchi, Y.; Yamaguchi, H.; Harada, A. *J. Am. Chem. Soc.* **2000**, *122*, 9876−9877.
(14) (a) Kunitake, M.; Kotoo, K.; Manabe, O.; Muramatsu, T.; Nakashima, N. *Chem. Lett.* **1993**, 1033−1036. (b) Harada, A.; Li, J.; Kamachi, M. *Chem. Commun.* **1997**, 1413−1414. (c) Murakami, H.; Kawabuchi, A.; Kotoo, K.; Kunitake, M.; Nakashima, N. *J. Am. Chem. Soc.* **1997**, *119*, 7605−7606.
(15) (a) Harada, A.; Kamachi, M. *Chem. Commun.* **1990**, 1322−1323. (b) Harada, A.; Kamachi, M. *Macromolecules* **1990**, *23*, 2821−2823. (c) Harada, A.; Li, J.; Kamachi, M. *Nature* **1992**, *356*, 325−327. (d) Harada, A.; Li, J.; Kamachi, M. *J. Am. Chem. Soc.*, **1994**, *116*, 3192−3196. (e) Harada, A.; Li, J.; Kamachi, M.; Kitagawa, Y.; Katsube, Y. *Carbohydr. Res.* **1998**, *305*, 127−129. (f) Harada, A. *Acta Polym.* **1998**, *49*, 3−17. (g) Okada, M.; Kamachi, M.; Harada, A. *J. Phys. Chem. B* **1999**, *103*, 2607−2613. (h) Kamitori, S.; Matsuzaka, O.; Kondo, S.; Muraoka, S.; Okuyama, K.; Noguchi, K.; Okada, M.; Harada, A. *Macromolecules* **2000**, *33*, 1500−1502. (i) Okada, M.; Kawaguchi, Y.; Okumura H.; Kamachi, M.; Harada, A. *J. Polym. Sci., Part A: Polym. Chem.* **2000**, *38*, 4839−4849.
(16) (a) Harada, A.; Li, J.; Kamachi, M. *Nature* **1993**, *364*, 516−518. (b) Harada, A.; Li, J.; Kamachi, M. *Nature* **1994**, *370*, 126−128. (c) Harada, A. *Acc. Chem. Res.* **2001**, *34*, 456−464.
(17) (a) Miyake, K.; Aiso, Y.; Komiyama, M.; Harada, A.; Kamachi, M.; Shigekawa, H. *Jpn. J. Appl. Phys.* **1994**, *33*, 3720−3722. (b) Yasuda, S.; Miyake, K.; Goto, Y.; Ishida, M.; Hata, K.; Fujita, M.; Yoshida, M.; Sumaoka, J.; Komiyama, M.; Shigekawa, H. *Jpn. J. Apply. Phys.* **1998**, *37*, 3844−3848. (c) Shigekawa, H.; Miyake, K.; Sumaoka, J.; Harada, A.; Komiyama, M. *J. Am. Chem. Soc.* **2000**, *122*, 5411−5412.
(18) Liu, Y.; Li, L.; Fan, Z.; Zhang, H.-Y.; Wu, X.; Guan, X.-D.; Liu, S.-X. *Nano Lett.* **2002**, *2*, 257−261.

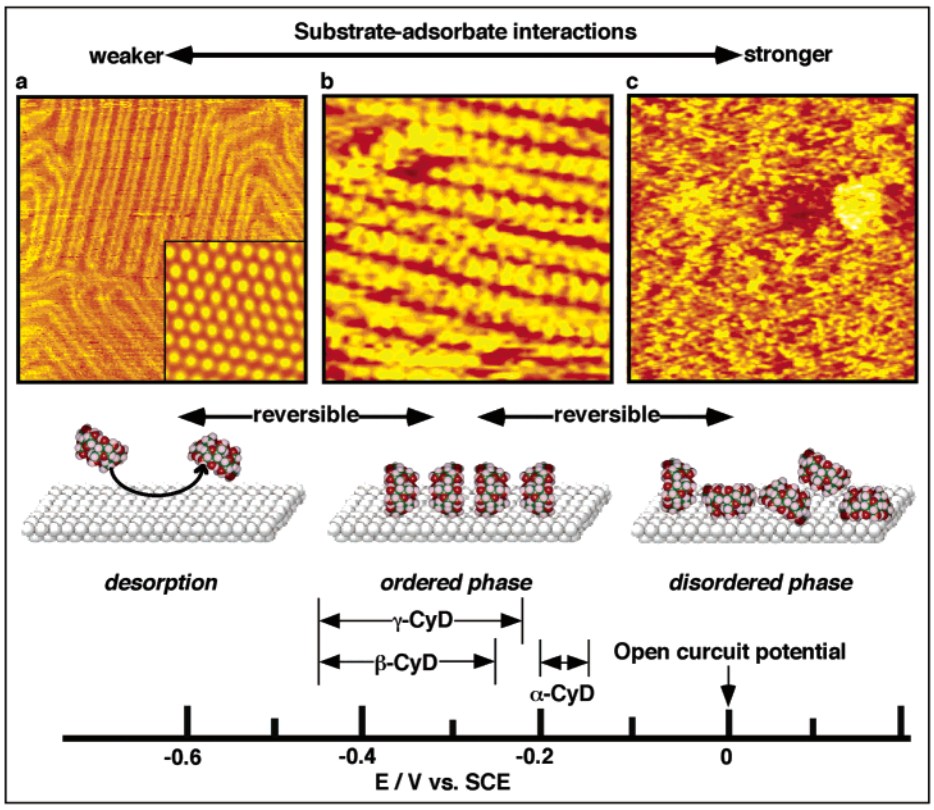

Figure 2. Electrode potential diagram for three states, (a) "desorption" state, (b) "ordered state", and (c) "disordered state", with corresponding schematic illustrations and typical STM images. (a) Tunneling current, $I_t = 2.4$ nA; tip potential, $E_t = +0.14$ V; and the electrode potential, $E_s = -0.60$ V. (b) $I_t = 2.4$ nA, $E_t = +0.14$ V, and $E_s = -0.45$ V. (c) $I_t = 1.6$ nA, $E_t = -0.13$ V, and $E_s = +0.10$ V. Each AISO potential range for the nanotubes formation of α-, *β*-, and *γ*-CyD is marked by the arrow.

E (Digital Instruments, Santa Barbara, California) and Pico-STM (Molecular Imaging Co. Ltd.) instrument. An Au(111) facet formed on a single-crystal bead was used for STM measurements. The tunneling tip was prepared from an electrochemically etched W wire, and its side wall was sealed with transparent nail polish to reduce the faradaic current. Several nail polished tips were kept in the water for more than 1 day to check the influence of impurities on the STM experiments. All images were collected in the constant current mode. The Au(111) electrodes were annealed in an H_2-O_2 flame and quenched in pure water saturated with H_2. The electrodes were transferred into an STM cell filled with 10 mM $NaClO_4$ aqueous solution containing CyD. Two Pt wires were used as reference and counter electrodes in the STM cell, respectively. All potentials are quoted with respect to a saturated calomel electrode (SCE).

3. Results and Discussion

3.1. CyD-Nanotube Formation by Potential-Controlled Adsorption. As we have reported in previous papers, the adsorption behaviors including the formation of nanotube structures of CyD's depended on the electrode potential.[6a,b] Figure 2 is a schematic representation of the electrode potential dependency for the adsorption of CyD's. At the open circuit potential (near +0.0 V), which corresponds to no potential control, the surface was totally covered by randomly adsorbed CyD's (Figure 2c). In the negative potential region, desorption of CyD's was observed. In this state, despite the presence of CyD's, the atomic lattice of Au(111) was observed. Therefore, CyD's are desorbed from the Au(111) surface at negative potentials, as shown in Figure 2a. The adsorption and desorption of CyD molecules were essentially reversible for all CyD's. At the specified midrange situated between these potentials, ordered molecular arrays with nanotube structures were formed on the Au(111) surface (Figure 2b). Formation of these ordered arrays under conditions where the substrate−adsorbate interaction was neither too strong nor too weak was termed "adsorption-induced self-organization" (AISO).

Generally, the coverage of neutral molecules is greatest at a potential of zero charge (PZC), and adsorption tended to be prevented onto the polarized surfaces.[10] It is plausible that the desorption of CyD on Au(111) at negative potentials is caused by the counterion in the electrolyte solution. The counterions in the electrolyte solution may approach and push out the adsorbates. As the electrode potential gradually moved toward PZC, CyD was adsorbed and nanotube structures were formed on the surfaces via rapid surface diffusion and acceleration of the adsorption/desorption equilibrium.[6,7] It has been reported that the adsorption of CyD onto a mercury electrode revealed the potential-induced transition of adsorption orientations by means of an electrochemical investigation.[19]

Interestingly, the range of potentials for AISO differed for each CyD. The potentials for AISO of α-, *β*- and *γ*-CyD, in which nanotube structures were formed, were from −0.15 to −0.20 V, from −0.25 to −0.45 V, and from −0.22 to −0.45 V, respectively. The AISO potential ranges for the formation of nanotubes are indicated by the arrows on the potential diagram in Figure 2. The AISO potential ranges for α-CyD were positive relative to those for *β*- and *γ*-CyD. This observation suggests that *β*- and *γ*-CyD require a more negative potential

(19) Jaworski, R. K.; Goledzinowski, M.; Galus, Z. *J. Electroanal. Chem.* **1988**, *252*, 425−440.

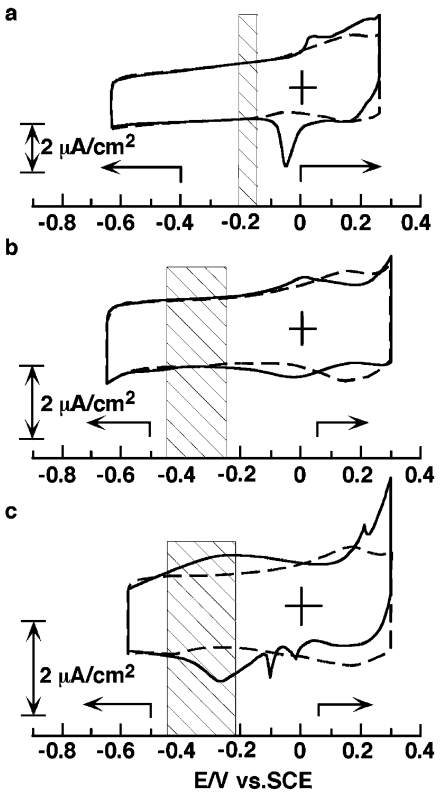

Figure 3. Cyclic voltammograms observed on Au(111) electrodes in 10 mM $NaClO_4$ in the absence (dotted line) and presence (solid line) of 2.0 μM CyD. (a) α-CyD, (b) β-CyD, and (c) γ-CyD. The scan rate of all measurements was 40 mV/s. The ranges of AISO potentials suitable for α-, β-, and γ-CyD to form nanotube structures are marked by slanted areas. The arrows on the potential scale bars, which are located on the left and right sides, indicate the potential regions for "desorption" and "random adsorption", respectively. Essentially, the same CVs resulted when the scan rate was slow, until 5 mV/s.

for AISO than α-CyD in order to weaken adsorption and induce self-organization. In another words, the adsorption strengths of β- and γ-CyD are stronger than that for α-CyD. This is likely attributable to the much bigger CyD ring sizes.

3.2. Comparison of Adsorption Behaviors for Cyclodextrins by Cyclic Voltammetry. Parts a−c of Figure 3 show cyclic voltammograms (CVs) of a bare Au(111) electrode in 10 mM $NaClO_4$ in the absence (dotted line) and presence (solid line) of 2.0 μM α-, β-, and γ-CyD, respectively. Each AISO potential region where the CyD-nanotube structures were observed is marked by slanted areas. In addition, each potential region for "desorption" and "random adsorption" are also marked by left- and right-hand arrows, respectively, in each part of the figure.At the negative potential ranges beyond the AISO regions in each system, the features of the CVs are in good agreement with those of the pure electrolyte solution. This suggests the desorption of CyD molecules from Au(111) over this range, as suggested by the STM imaging results. Jarzabek has described the adsorption of β-CyD's onto a polycrystalline Au electrode in terms of electrochemical capacitance.[20] The difference in capacitance between the presence and the absence of CyD's becomes smaller toward more negative potentials, and the capacitance for both systems is almost equal at the negative potential region near −1.0 V versus SCE. This indicates that the coverage of CyD decreased with the lowering of the potential

(20) Jarzabek, G. *J. Electroanal. Chem.* **1990**, *294*, 253−265.

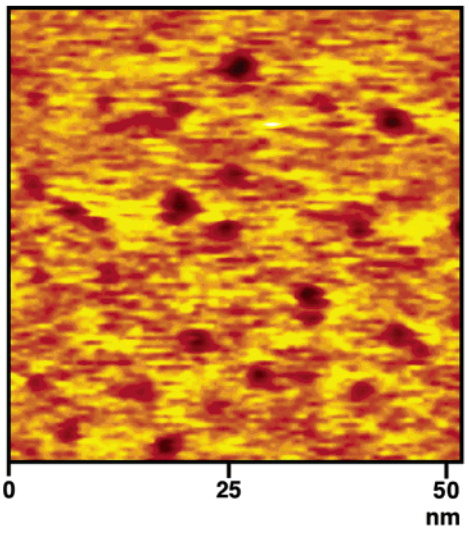

Figure 4. Typical STM image of Au(111) surface roughened by pit formation observed at the positive potential side from OCP in 10 mM $NaClO_4$ in the presence of 2.0 μM α-CyD. The image was obtained at I_t = 1.0 nA, E_t = −0.13 V, and E_s = +0.10 V.

until finally the desorption of CyD occurred. These observations are in agreement with our results.

On the contrary, at the positive potentials beyond the AISO regions, the features of CVs are entirely different from those observed in the absence of CyD's. This indicates the adsorption of CyD's onto the Au(111) over this range of potentials. At the AISO regions, α- and β-CyD revealed almost the same CV curves as those in the absence of CyD, although STM observation clearly demonstrated adsorption and self-organization. These observations indicate that the time scale for the CV was too short to show self-organization of α- and β-CyD. Interestingly, γ-CyD gave broad peaks, which might be due to the capacitance change caused by adsorption but not electron transfer, at the region.

Moreover, at the positive potential region beyond the open circuit potential (OCP), the oxidation of CyD's and the desolation of Au surfaces occurred simultaneously, effectively complicating electrochemical behaviors and surface morphologies. The oxidative and reductive peaks observed at the positive potentials beyond +0.1 V could be attributed to oxidation and the subsequent reduction of CyD's. Jarzabek also mentioned the oxidation of β-CyD on an Au electrode.[20] Figure 4 shows the typical desolation of flat terraces by the formation of small Au pits observed at +0.1 V. Note that the intact Au terraces can be observed at the same potential in pure electrolyte solution without CyD.

These results obviously indicate that the AISO potential region where the nanotube structures were induced is located at the midrange between the desorption and saturated adsorption. No remarkable peaks indicating phase transitions such as "order−disorder" or "adsorption−desorption" are observed.

3.3. Comparison of Nanotube Structures of α-, *β*-, and *γ*-Cyclodextrins. Parts a−c of Figure 5 show the STM images of self-organized nanotube structures of α-, β-, and γ-CyD's under AISO conditions. Each CyD molecule covered the surfaces as nanotube structures, which could be clearly visualized over a relatively wide region. Interestingly, the surface morphology of the CyD nanotube for α-CyD was different from those for β- and γ-CyD. Figure 5a shows typical α-CyD-

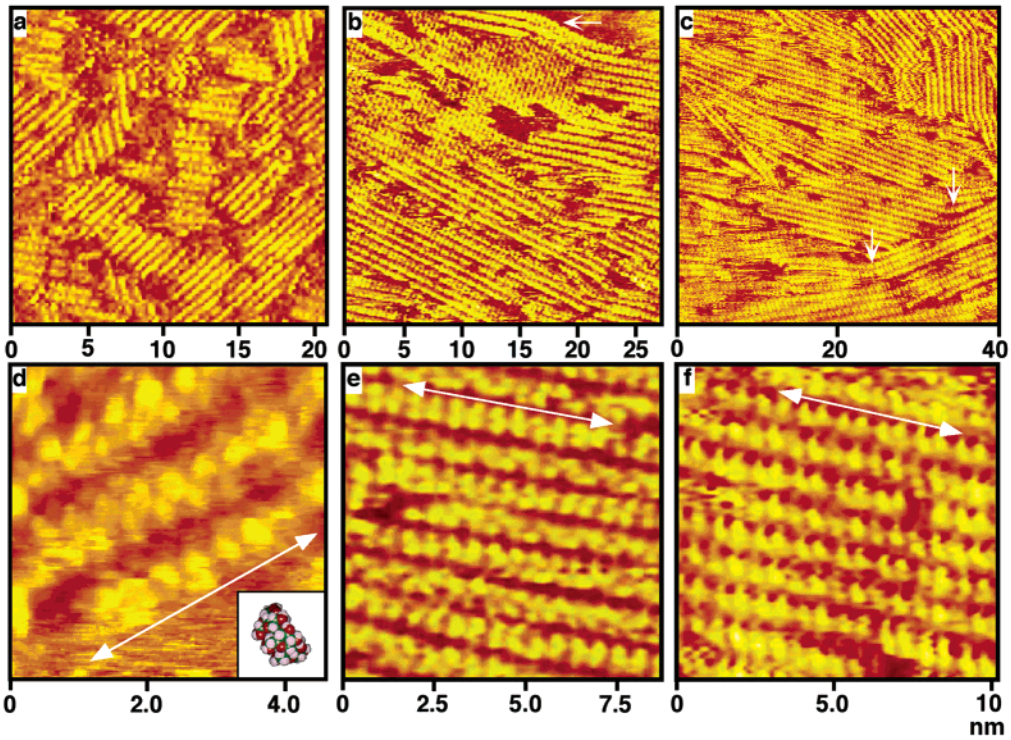

Figure 5. High-resolution STM images of CyD-nanotube arrays on Au(111) surfaces for α-CyD ((a) 22 nm × 22 nm, $I_t = 1.0$ nA, $E_t = +0.16$ V, and $E_s = -0.20$ V; (d) 4.6 nm × 4.6 nm, $I_t = 0.81$ nA, $E_t = +0.14$ V, and $E_s = -0.15$ V), for β-CyD ((b) 28 nm × 28 nm, $I_t = 2.4$ nA, $E_t = +0.14$ V, and $E_s = -0.45$ V; (e) 8.7 nm × 8.7 nm, $I_t = 2.4$ nA, $E_t = +0.14$ V, and $E_s = -0.45$ V), and for γ-CyD ((c) 40 nm × 40 nm, $I_t = 1.6$ nA, $E_t = +0.04$ V, and $E_s = -0.35$ V; (f) 10.2 nm × 10.2 nm, $I_t = 2.1$ nA, $E_t = +0.04$ V, and $E_s = -0.35$ V). The solution was 10 mM $NaClO_4$ in the presence of 2.0 μM CyD. The inset in part d shows a space filling model of α-CyD, which possesses the same orientation as that in the STM image. The arrows in parts d−f reveal the running direction of the nanotubes.

nanotube structures with triangular arrangements. As mentioned in the previous article,[6a] the triangular arrangement of nanotubes is due to the long-distance lattice match between molecular adlayers and Au lattices, indicating that the α-CyD nanotube possesses an epitaxial arrangement.

On the other hand, the lengths of nanotubes formed from β- and γ-CyD were longer than that from α-CyD, as shown in Figure 5b and c, respectively. Furthermore, the direction of the β- and γ-CyD nanotubes did not seem to be regulated by the underlying Au(111) lattices in contrast with the arrangements of the α-CyD nanotubes. This suggests that the intermolecular interactions for β- and γ-CyD are stronger than those for α-CyD. As we mention later, the dominant source of intermolecular interactions to form nanotubes are hydrogen bonds between hydroxyl groups on both side faces of the CyD's. The intermolecular interactions are, therefore, roughly proportional to the number of glucose units in each CyD molecule. Interestingly, turns of nanotubes can be frequently seen in Figure 5b and c, as indicated by arrows. Such turns were rarely observed for α-CyD. This may also be due to the stronger intermolecular interactions and the softness of the β- and γ-CyD relative to those of α-CyD.

It is worth emphasizing that "nanotube" structures on surfaces are formed not from simple epitaxy but from the self-organization of molecules. Structures of the molecular adlayers are controlled by the balances between the substrate−adsorbate interactions and the intermolecular interactions, as shown in Figure 1. When the substrate−adsorbate interaction is dominant and the intermolecular interaction is relatively weak, the adlayer would possesse simple epitaxy. By contrast, when the intermolecular interaction is dominant, the self-organized adlayer will appear as incommensurate adlayers, which seems not to be influenced by the substrate, like "nanotubes" of β- and γ-CyD. Moreover, if both the interactions are well balanced, the commensurate and self-organized adlayers, such as triangular arrangements of α-CyD nanotubes and a network structure of trimesic acid,[7] will appear.

High resolution STM imaging clearly gives not only the information regarding nanotube arrangements on the surfaces but also information regarding the molecular shape and arrangement of the individual molecules within the nanotubes. Parts d−f of Figure 5 show high-resolution STM images of the self-organized nanotubes of α-, β-, and γ-CyD over relatively narrow areas, respectively. The arrows in the parts of the figure are along the nanotube structures. Typically, each CyD molecule can be recognized as a rectangular bright spot in Figure 5e for β-CyD. This indicates that the cavities of CyD's are parallel to the surface and that the molecules would be connected to each other in a "head-to-head" and "tail-to-tail" fashion to form the nanotube. A similar arrangement of CyD molecules has been reported for polyrotaxane.[15,16]

The dominant driving forces for the formation of the tube structure are the intermolecular H-bond interactions among hydroxyl groups on the same side faces of CyD molecules. The same intermolecular interaction is at work in the formation of polyrotaxane. In addition, the sideways orientation would only be stable in a "nanotube" structure but not in "isolated" adsorption.[6b] Therefore, the specific orientation of the molecules proves the nanotube structure is the result of the self-organization of CyD's, not simple adsorption.

The observed distances between rectangular features along the tube were 0.6 ± 0.1 nm, which were essentially constant

for the series of CyD's. These values are consistent with the expected height (Scheme 1, Y) of CyD's along the cavity but are too short for the diameter of CyD's (Scheme 1, X) with an upward orientation. In contrast, the interval distances between regularly aligned parallel tubes were estimated as 0.9 ± 0.1 nm, 1.0 ± 0.1 nm, and 1.1 ± 0.1 nm, for α-, β-, and γ-CyD, respectively. The sizes are consistent with the value expected from the chemical models. For α-CyD, a corresponding distance of 1.0 nm has been reported as the measured periodical value for the honeycomb crystal of α-CyD complexes with hexa(ethyleneglycol) or tetra(ethyleneglycol)dibromide by means of an X-ray diffraction study.[15e]

High-resolution images occasionally obtained allowed visualization of the inner structure of CyD as shown in Figure 5d. In the image, three α-CyD nanotubes are shown running from the upper right direction to the lower left. Each molecule seems to consist of three spots, which might correspond to glucose moieties.

3.4. Dynamic Observation of Adsorption Behaviors of Cyclodextrins. As mentioned previously, the adsorption behaviors, including the formation of nanotube structures of CyD's, are dependent on the electrode potential. As one of its biggest advantages, the in situ scanning probe technique allows observation of these dynamic processes in the solution including such processes, the self-ordering, and the destruction of the nanotube structure.[6b] Other reported examples of in situ STM visualization of phase transition processes are an "order−disorder" transition for 2,2′-bipyridine on Au(111)[1b,9a,c] and "order−order" transitions for uracil on Au(111),[9d] ethanethiol adlayers on Au(100),[9e] and trimesic acid on Au(111).[7]

Parts a and b of Figure 6 show typical sequential STM images for the self-organization process for an α-CyD nanotube. The potential was initially set at −0.40 V, where the CyD molecule did not adsorb. An intact reconstructed surface was then observed. When the electrode potential jumped to −0.20 V, the typical herringbone type double row reconstruction disappeared and, simultaneously, nanotubes started to appear. The domain consisting of nanotubes gradually covered the Au(111) surface. In Figure 6a, which was obtained 2 min after the potential shift, the domain consisting of nanotubes can be seen in the lower terrace on the left side of the image. However, on the right side of the lower terrace in the middle portion of the image, there is no nanotube domain. After approximately a 30 s interval, the surface was entirely covered in nanotubes, as shown in Figure 6b. A small Au island and a protrusion of the upper terrace are markers to prove observations were made at the same place. Interestingly, the domain of the nanotube structures formed independent of a step line on the Au surface.

In a previous paper, we reported the phase transition from an ordered phase (β-CyD nanotube) to a disordered one.[6b] The potential jumped from the AISO range to the OCP. After the potential was positively shifted to the OCP, each nanotube shortened gradually with time. Simultaneously, many protrusions of randomly adsorbed β-CyD molecules started to appear out of the ordered structures. Approximately 6 min. after the potential shift, the surface was entirely covered by randomly adsorbed β-CyD molecules. This observed "order-to-disorder" transition indicates that the ordered adlayer of β-CyD is stable only over a particular potential range and that the balance of the various interactions is thermodynamically delicate. Note that the solution conditions such as concentration and temperature are also directly related to this balance, because such parameters influence the adsorption−desorption equilibrium of CyD.

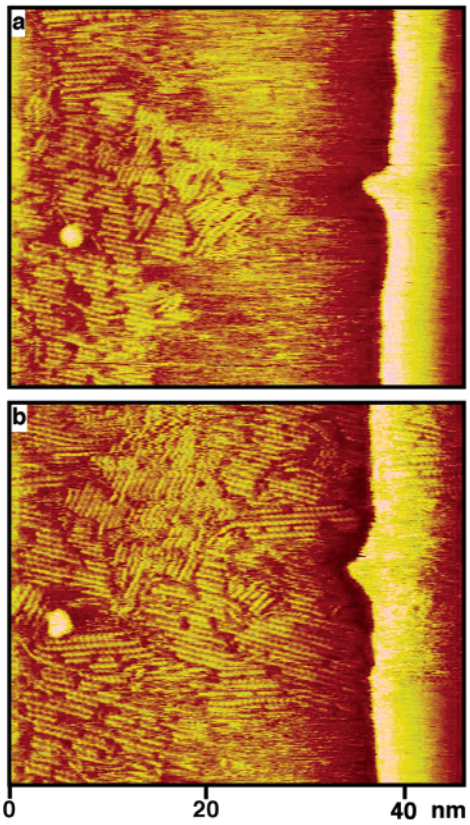

Figure 6. Sequential STM images of the self-organization process of α-CyD. The images were collected at 2 min (a) and 2.5 min (b) just after changing the potential from −0.40 to −0.20 V in 10 mM $NaClO_4$ solution in the presence of 2.0 μM α-CyD. (a) 48 nm × 48 nm, $I_t = 2.5$ nA, $E_t = -0.00$ V, and $E_s = -0.20$ V; (b) 48 nm × 48 nm, $I_t = 2.4$ nA, $E_t = +0.06$ V, and $E_s = -0.20$ V.

Next, the desorption of CyD from the nanotube phase, the potential jump from the AISO region to the negative region, was examined. Basically, the adsorption and desorption equilibrium of CyD's was reversible, and the intact reconstructed surface was observed again when the potential was set to negative. Figure 7 shows sequential STM images of the desorption process from α-CyD nanotubes just after the potential jumped from −0.20 to −0.45 V, at which the reconstructed surface is observed. Each nanotube shortened gradually with time, and the reconstructed surface began to be observed. Arrays of α-CyD nanotube and the reconstructed surface areas temporarily coexisted, as shown in Figure 7a. The reconstructed $(\sqrt{3} \times 23)$-Au(111) surfaces appeared in open spaces after the nanotube array had disappeared. In addition, the running directions $[11\bar{2}]$ of nanotubes and the herringbone type double rows of reconstructed surfaces were essentially the same. This observation reveals that α-CyD nanotubes possess epitaxial arrangements.

Parts b and c of Figure 7 were collected at the same place approximately 1 min and 4 min after the potential jump, respectively. In Figure 7c, nanotube domains were decreased on the surface compared with those in Figure 7b. Interestingly, the islands of nanotubes which ordered in a parallel arrangement moved around on the surface. For example, the running direction of nanotubes in the array located at the right portion, with the

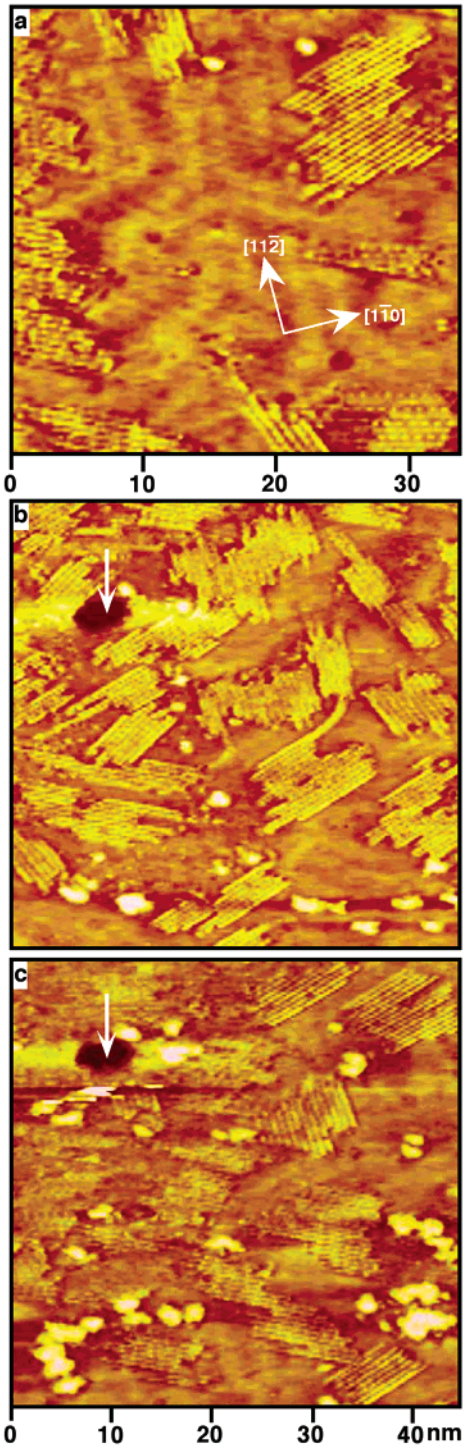

Figure 7. Sequential STM images of the desorption process of α-CyD collected at 1 min (b) and 4 min (a, c) after the potential was changed from −0.20 to −0.45 V in 10 mM $NaClO_4$ solution in the presence of 2.0 μM α-CyD. (a) 33 nm × 33 nm, $I_t = 2.0$ nA, $E_t = -0.02$ V, and $E_s = -0.45$ V; (b) 45 nm × 45 nm, $I_t = 2.0$ nA, $E_t = -0.02$ V, and $E_s = -0.45$ V; and (c) 45 nm × 45 nm, $I_t = 2.0$ nA, $E_t = -0.02$ V, and $E_s = -0.45$ V. The arrows indicate the pit created by the tip and used as a location marker.

big pit as a marker (marked by arrow) in Figure 7b, was different from that in the array in the same region in Figure 7c. It also proves the weak adsorption of molecules at AISO condition.

3.5. Selective Adsorption of γ-CyD from a Solution Also Containing α-CyD. As mentioned previously, the AISO potential regions for α-CyD were positively located relative to

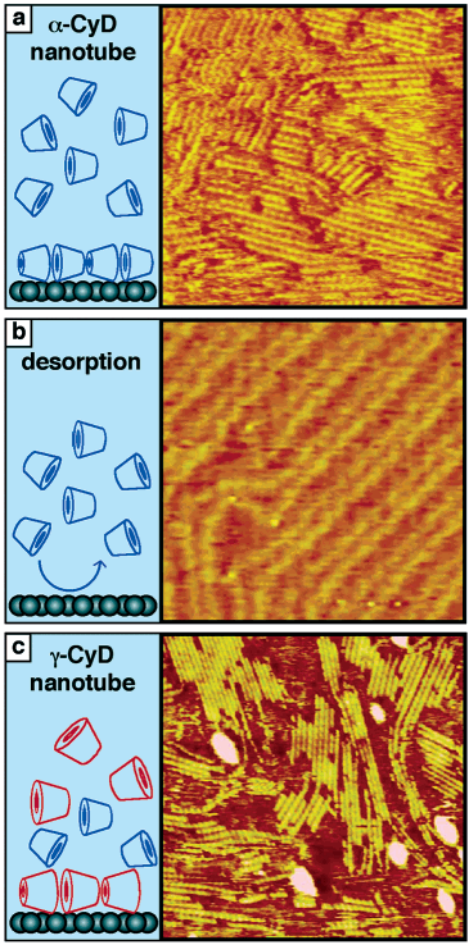

Figure 8. Sequential STM images for selective adsorption of γ-CyD from an α-CyD and γ-CyD mixture solution. The "α-CyD-nanotube" image ((a) 25 nm × 25 nm, $I_t = 2.5$ nA, and $E_t = 0.00$ V) was collected at −0.20 V in 10 mM $NaClO_4$ in the presence of 2.0 μM α-CyD. The "reconstructed" surface image ((b) 25 nm × 25 nm, $I_t = 2.0$ nA, and $E_t = -0.05$ V) was obtained 6 min after the potential jump from −0.20 V to −0.40 V to desorb α-CyD molecules. The typical "γ-CyD-nanotube" image ((c) 34 nm × 34 nm, $I_t = 2.0$ nA, and $E_t = +0.03$ V) was obtained 5 min after the injection of the γ-CyD stock solution at −0.40 V. The final concentration of the α-CyD and γ-CyD solution was approximately 2.0 μM.

those for β- and γ-CyD. This suggests that the adsorption strengths of β- and γ-CyD are stronger than that for α-CyD. Therefore, the possibility of selective adsorption from mixed CyD solutions by means of precise electrode potential control was anticipated.

The selective adsorption of γ-CyD from a mixed solution containing α-CyD was conducted according to the following procedure. The electrode potential was initially set to −0.40 V in order to start with an intact Au(111) electrode in the electrolyte solution in the presence of α-CyD. After observation of the reconstructed surface, the potential was gradually moved to −0.20 V to establish α-CyD nanotubes (Figure 8a). The typical epitaxial arrangement for the α-CyD array was observed, as shown in Figure 8a. The potential was moved back to −0.40 V for the desorption of α-CyD. The reconstructed surface appeared again (Figure 8b). Then, a high concentration of γ-CyD stock solution was added to the solution to equal a concentration of 2.0 μM under the potential control at −0.40 V. After the mixing in of γ-CyD's, the nanotube array was found to be reformed without a positive potential shift, as shown in Figure 8c.

The reformed array revealed a thoroughly different arrangement of nanotubes compared to that for α-CyD (Figure 8a). The average length of the reformed nanotube was longer, and the interval distance of adjacent nanotubes was 1.1 ± 0.1 nm. All results clearly indicate that γ-CyD nanotubes were reformed by electrochemical selective adsorption, proving that the adsorption strength of γ-CyD is stronger than that for α-CyD.

4. Conclusions

Details of the adsorption behaviors of α-, β-, and γ-CyD on Au(111) were described with the observation of dynamic processes, such as self-ordering, order-to-disorder, and order-to-desorption. Essentially the same dynamic processes were observed for α-, β-, and γ-CyD. These results prove that suitable AISO conditions are based on well-balanced interactions and that precise control of the electrode potential makes it possible to control this delicate interaction balance. Electrochemically controlled adsorption for AISO has been proven to work not only for CyD's but also for various other molecules. The combination of AISO and in situ STM observation is a key technique for construction and research of 2D supramolecular structures on surfaces by the "wet process". The construction of 2D molecular architectures will lead to "bottom up"-type nanoscience and nanochemistry in the future.

Acknowledgment. This work was supported by CREST (Core Research for Evolutional Science and Technology) of JST (Japan Science and Technology Corporation).

JA021351B